REGULAR ARTICLE

DFT-steric-based energy decomposition analysis of intermolecular interactions

**Dong Fang · Jean-Philip Piquemal ·
Shubin Liu · G. Andrés Cisneros**

Abstract Application of a novel energy decomposition analysis (EDA) based on the recently introduced density functional theory (DFT) steric analysis is presented. The method is compared with results from the constrained space orbital variations (CSOV) and Bader's quantum theory of atoms in molecules (QTAIM) topological analysis. These two analyses explain the driving forces for the formation of dimers from different perspectives. The components of the DFT steric analysis are shown to have good linear relationships with the total interaction energy for hydrogen-bonding dimers. It is observed that some components from the new EDA method, such as steric energy, favor the formation of dimers. Moreover, comparison of the different contributions between CSOV and the DFT steric analysis provides additional insights into the physical meaning of the respective components. In addition to the total interaction energy, DFT steric energy has been found to correlate with the electron density at critical points from QTAIM analysis in different patterns for different molecular systems, which qualitatively accounts for the linear relationships between the steric and total interaction energy. The DFT steric energy is found to represent effects arising from the spatial arrangement of the electron density when dimers form, reminiscent of the steric effects invoked in chemical systems.

Keywords DFT steric · CSOV · QTAIM

D. Fang · G. A. Cisneros (✉)
Department of Chemistry, Wayne State University, Detroit,
MI 48202, USA
e-mail: andres@chem.wayne.edu

J.-P. Piquemal
Univ. Paris 06, UMR 7616 Laboratoire de Chimie Théorique,
UPMC, Sorbonne Universités, Case Courrier 137, 4 Place
Jussieu, 75005 Paris, France

J.-P. Piquemal
UMR 7616, Laboratoire de Chimie Théorique, CNRS, Case
Courrier 137, 4 Place Jussieu, 75005 Paris, France

S. Liu (✉)
Research Computing Center, University of North Carolina at
Chapel Hill, Chapel Hill, NC 27599-3420, USA
e-mail: shubin@email.unc.edu

1 Introduction

The accurate determination of intermolecular interactions, such as hydrogen bonding, π–π stacking, has attracted a lot of attention due to its importance in determining the physical and chemical properties of molecular systems, especially biomolecules. Various energy decomposition methods have been proposed for the purpose of understanding the physical meanings of these interactions more deeply, which is especially helpful in the development of force fields [1–20]. The energy decomposition methods can be roughly categorized into perturbative and variational ones. Among the perturbative methods, one of the widely used methods is the symmetry-adapted perturbation theory (SAPT) [8], in which the Hamiltonian is divided into Fock operators, the fluctuation potential for each monomer and the interaction potential. Physically, meaningful components such as electrostatic, exchange repulsion, induction, and dispersion can be obtained. Recently, density functional theory (DFT)-based SAPT methods have also been developed [12]. In the case of variational methods, several approaches have been proposed. The first such method was

the Kitaura–Morokuma (KM) energy decomposition scheme [3]. Subsequently, a variety of new approaches that improve on the KM method have been proposed including the natural energy decomposition (NEDA) [7], the reduced variational space (RVS) analysis [6], the localized molecular orbital energy decomposition analysis (LMO-EDA) [17], the constrained space orbital variation (CSOV) [5, 21], the absolutely localized molecular orbitals energy decomposition analysis (ALMO-EDA) [13, 20, 22], and the block-localized wave function energy decomposition [10, 19] to name a few. Some of these methods can only be applied to Hartree–Fock (HF) wave functions, while others can be employed with post-HF methods. Some of these approaches have been extended to DFT using Kohn–Sham orbitals. In addition, DFT-based EDA methods have been developed as well, for example, fragment-localized Kohn–Sham orbitals via a single CI procedure [15] and the density-based energy decomposition with variationally determined intermediate state energies [18].

Recently, one of us has (SL) proposed the concept of DFT steric energy [14] in order to quantify the concept of steric effect, which is widely used in chemistry. It has been applied to a variety of systems to study conformational changes [23], the anomeric effect [24], and chemical reactions [25]. In this contribution, we present an extension of DFT sterics to develop a novel EDA method, DFTs–EDA. This new DFTs–EDA method is applied to several molecular dimers, and the results are compared with results obtained from CSOV decomposition analysis and QTAIM topological analysis [26] to gain a better understanding of the physical meanings of its components. The organization of the paper is as follows: in the following section, we introduce the theory for DFT steric and CSOV decomposition analyses. Subsequently, results for several molecular systems comprising 24 hydrogen-bonded water-containing dimers, DNA base pairs, and two types of benzene dimers are presented and discussed, followed by the conclusion section.

2 Theory and methodology

2.1 DFT steric analysis

In DFT, the total energy is expressed as

$$
\begin{aligned}
E[\rho(\mathbf{r})] &= T_s[\rho(\mathbf{r})] + E_e[\rho(\mathbf{r})] + E_{XC}[\rho(\mathbf{r})] \\
&= T_s[\rho(\mathbf{r})] + E_e[\rho(\mathbf{r})] + E_X[\rho(\mathbf{r})] + E_C[\rho(\mathbf{r})],
\end{aligned} \quad (1)
$$

where T_s, E_e, and E_{XC} are the noninteracting kinetic, electrostatic, and exchange–correlation energies, respectively. The final term can be further separated into exchange (E_X) and correlation (E_C) components.

Recently, Liu has proposed a different partition method of the total energy [14]:

$$
E[\rho(\mathbf{r})] = E_s[\rho(\mathbf{r})] + E_e[\rho(\mathbf{r})] + E_q[\rho(\mathbf{r})], \quad (2)
$$

where $E_s[\rho(\mathbf{r})]$ is defined as the steric energy, $E_e[\rho(\mathbf{r})]$ is the same Coulomb energy term in Eq. 1, and $E_q[\rho(\mathbf{r})]$ represents the energy contributions from quantum effects due to the exchange–correlation effects. The first term is equal to the Weizsäcker kinetic energy [27]:

$$
E_s[\rho(r)] = T_w[\rho(r)] = \frac{1}{8} \int \frac{|\nabla \rho(r)|^2}{\rho(r)} dr \quad (3)
$$

The last term in Eq. 2 is defined as

$$
E_q[\rho(\mathbf{r})] = E_{XC}[\rho(\mathbf{r})] + E_{Pauli}[\rho(\mathbf{r})], \quad (4)
$$

where $E_{Pauli}[\rho(\mathbf{r})]$ represents the Pauli repulsion:

$$
E_{Pauli}[\rho(\mathbf{r})] = T_s[\rho(\mathbf{r})] - T_w[\rho(\mathbf{r})]. \quad (5)
$$

For a bosonic system, the kinetic energy will become $T_w[\rho(\mathbf{r})]$. For fermions such as electrons, after excluding $E_{Pauli}[\rho(\mathbf{r})]$, $E_e[\rho(\mathbf{r})]$, and $E_{XC}[\rho(\mathbf{r})]$, the remaining term, $T_w[\rho(\mathbf{r})]$, should be a measure of steric effects, which is related to the spatial distribution of the electron density.

Applying this scheme to investigate interaction energies leads to following formulas:

$$
\begin{aligned}
\Delta E[\rho(\mathbf{r})] &= \Delta T_s[\rho(\mathbf{r})] + \Delta E_e[\rho(\mathbf{r})] + \Delta E_{XC}[\rho(\mathbf{r})] \\
&= \Delta T_s[\rho(\mathbf{r})] + \Delta E_e[\rho(\mathbf{r})] + \Delta E_X[\rho(\mathbf{r})] + \Delta E_C[\rho(\mathbf{r})]
\end{aligned} \quad (6)
$$

and

$$
\begin{aligned}
E_{tot}[\rho(\mathbf{r})] &= \Delta E[\rho(\mathbf{r})] \\
&= \Delta E_s[\rho(\mathbf{r})] + \Delta E_e[\rho(\mathbf{r})] + \Delta E_q[\rho(\mathbf{r})]
\end{aligned} \quad (7)
$$

where for the terms with Δ, their values are obtained by subtracting the sum of the corresponding term for monomers from the one for the molecular complex.

It should be noted that the DFT steric effect is an indication of the size of the system, which is verified quantitatively by the linear relationship between the Fisher information. The Fisher information is 1/8 of DFT steric effect, and the molecular and atomic volumes [28]. Therefore, a large negative value of the DFT steric effect means the dimer occupies less space than the sum of the monomers. Since no physical observable variable is directly linked to the steric effect, the definition of steric effect is not unique and may be different in some other approaches [29–31]. Thus, the DFT steric effect, which represents spatial effects, is slightly different from the common concept of the steric effect, which also includes some effects related to the Pauli exclusion.

2.2 Constrained space orbital variation

The constrained space orbital variation (CSOV) method [5, 32–35] decomposes the intermolecular interaction energy into four components: Coulomb, exchange repulsion, polarization, and charge transfer. The first two, namely Coulomb and exchange repulsion, are termed the frozen-core contribution since they involve unperturbed orbitals for the interacting monomers. The last two terms correspond to the induction effects allowing selected relaxation of the variational spaces.

$$
\begin{aligned}
E_{\text{tot}} &= E_{\text{FC}} + E_{\text{Pol}} + E_{\text{CT}} \\
&= E_{\text{Coul}} + E_{\text{Exch-Rep}} + E_{\text{Pol(A)}} + E_{\text{Pol(B)}} + E_{\text{CT(A}\to\text{B)}} \\
&\quad + E_{\text{CT(B}\to\text{A)}}
\end{aligned}
\tag{8}
$$

Following the Kitaura–Morokuma scheme, the frozen-core energy (E_{FC}) is calculated as the antisymmetrized Hartree product of the isolated monomer wave functions. When executing the SCF procedure, the occupied orbitals of monomers A and B remain frozen, which means there is no relaxation into the virtual orbitals. E_{Coul} corresponds to the classic Coulomb interaction, which includes the electron–electron repulsion, the electron-nucleus attraction, and the nucleus–nucleus repulsion. For the interactions involving electrons, the unperturbed molecular orbitals of monomers are used. The difference between E_{FC} and E_{Coul} is defined as the exchange repulsion term, which arises from the Pauli exclusion principle. It is worth noting that the CSOV values for E_{Coul} and $E_{\text{Exch-Rep}}$ are identical to the Coulomb and exchange terms obtained from the Kitaura–Morokuma decomposition if computed at the same level of theory.

The remaining terms, polarization (E_{Pol}) and charge transfer (E_{CT}), depend on the variation of the molecular orbitals and their eigenvalues in different variational space. For example, $E_{\text{Pol(A)}}$ is the energy due to the relaxation of the occupied orbitals of molecule A in the electric field generated by molecule B. When performing the SCF procedure on molecule A, molecule B's occupied orbitals are kept frozen and its virtual orbitals are not included in the variational calculation. During the procedure, molecule A's orbitals are orthonormal to the frozen MOs of B. A similar procedure is carried out in order to calculate $E_{\text{CT(A}\to\text{B)}}$. However, this time the virtual orbitals of B are allowed to relax so that the electrons can be transferred from A to B. Antisymmetrized wave functions are used in the calculations on both polarization and charge-transfer components to eliminate short-range problems in dimers concerning strong polarizing fields, which are known to produce artifacts in the original Kitaura–Morokuma decomposition. For DFT, Kohn–Sham orbitals are used in CSOV calculations by following the procedure above.

2.3 Non-covalent interaction (NCI) analysis

NCI [36] has been developed to visualize the non-covalent interaction by plotting the electron density versus the reduced density gradient. The peaks at low electron density characterize the desired non-covalent interaction. By multiplying the density by the sign of the second density Hessian eigenvalue ($\lambda2$), different types of interactions (attraction and repulsion) can be distinguished. Hence, it is a powerful tool to study the hydrogen bonding, which is classified as non-covalent attractive interaction. For NCI surfaces, red color is a sign of strong repulsion; blue color indicates strong attraction such as hydrogen bonding; and green color means weak interaction.

2.4 Computational details

The geometries of the dimers presented in this work were optimized with B3LYP [37, 38] /6-31G(d) level using the Gaussian 09 software suite [39]. The monomers were kept rigid in their respective monomer-optimized geometries during the geometry optimization of the dimers. Based on these optimized geometries, Kohn–Sham orbitals were obtained at the B3LYP level with two different basis sets, 6-31G(d) and 6-311++G(2d,2p), for subsequent EDA analysis for hydrogen-bonded water-containing dimers. All reported corrections to supermolecular energies for basis set superposition error (BSSE) use the counterpoise method [40]. CSOV energy decomposition was performed at the same level of theory (B3LYP/6-31G(d) and 6-311++G(2d,2p)) using a modified version of the Hondo program [41]. Density functional steric energy decomposition was done by a modified version of NWChem [42]. For the benzene dimers and DNA base pair, only the 6-31G(d) basis was considered. The AIMPAC program was used to calculate the critical points for AIM analysis. NCI surfaces were generated by the NCIPLOT program [43] with its default parameters and visualized using VMD [44].

3 Results and discussion

3.1 Hydrogen-bonding dimers: water-containing dimers and DNA base pair

Figure 1 shows all the 24 hydrogen-bonded water-containing dimers that have been studied in this paper and their NCI surfaces. The dimers include formamide–water, *N*-methylformamide–water, methanol–water, fluomethane–water, dichloromethane–water, difluoromethane–water, methane–water, ammonia–water, methylamine–water, and water–water. The results for the interactions obtained with
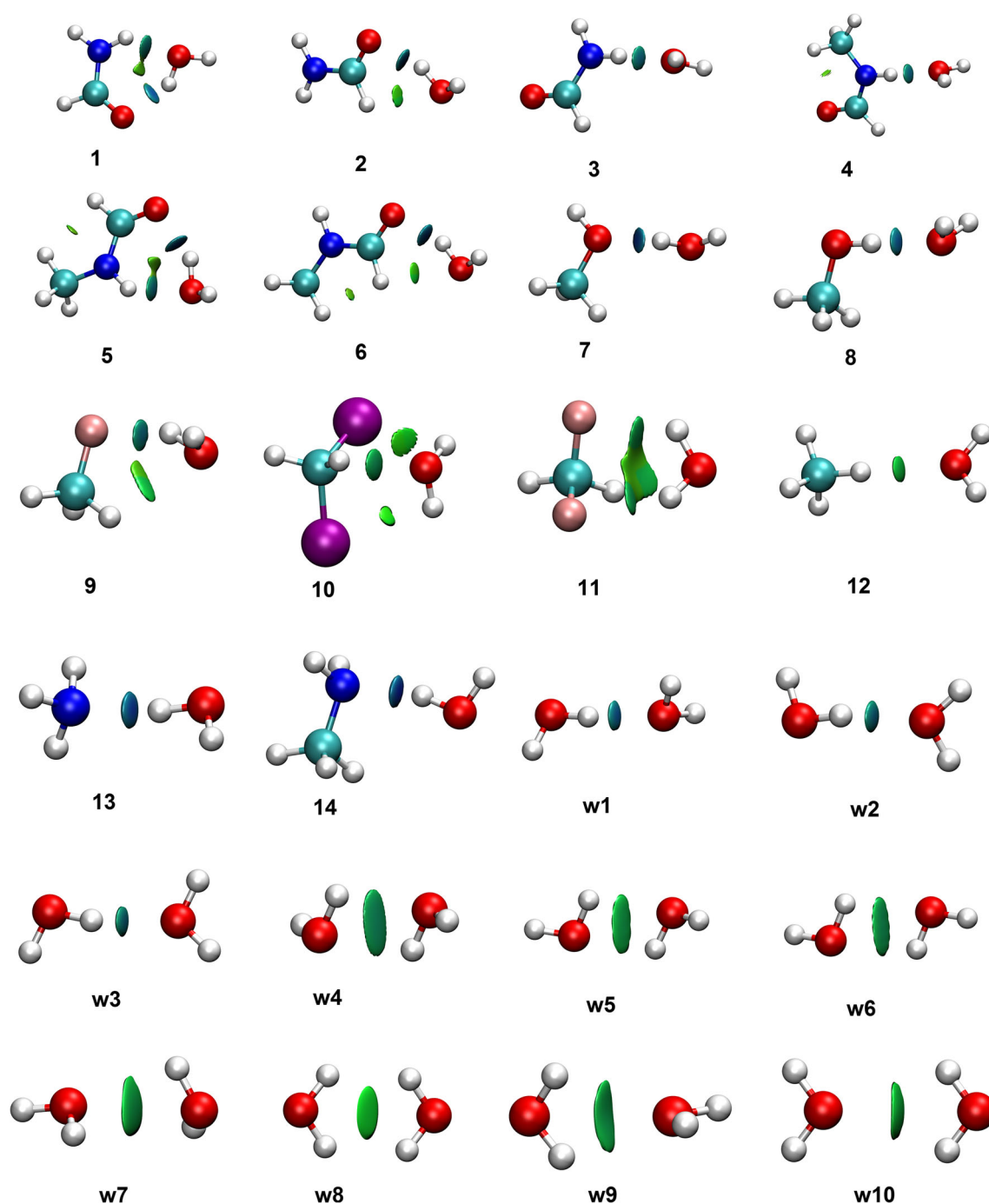
Fig. 1 NCI plots and structures of 24 dimers (The molecule on the left is A, and the right one is B.) The isovalue for NCI surfaces is 0.5 au. The surfaces are *colored* on a *blue–green–red* scale with -0.04 au $< \text{sing}(\lambda 2)\rho < 0.04$ au. (dimer *1, 2, 3*: formamide–water; dimer *4, 5, 6*: N-methylformamide–water; dimer *7, 8*: methanol– water; dimer *9*: fluomethane–water; dimer *10*: dichloromethane-water; dimer *11*: difluoromethane–water; dimer *12*: methane–water; dimer *13*: ammonia–water; dimer *14*: methylamine–water; dimer *w1–w10*: water–water)

the 6-311++G(2d,2p) basis sets are shown in Tables 1 and 2 (the results for 6-31G(d) are listed in Tables S1 and S2 in the Supporting Information). As shown in Table S3, it is well known [45] that the BSSE energies play an important role in the intermolecular interaction and this effect is reduced with a larger basis set. After taking the BSSE corrections into account, the difference between the total interaction energies given by the two basis sets is reduced to an average of 1.0 kcal/mol. Comparison of the corresponding components calculated using these two different

Table 1 CSOV decomposition on water-containing dimers (unit: kcal/mol; B3LYP/6-311++G(2d,2p))

Dimers	E_{FC}	E_{Coul}	$E_{Exch-Rep}$	E_{PolA}	$E_{CT(A \to B)}$	E_{PolB}	$E_{CT(B \to A)}$	E_{tot}
1	−2.2	−16.4	14.3	−1.4	−2.3	−1.0	−1.5	−8.3
2	−2.1	−10.1	8.0	−0.9	−2.2	−0.5	−0.3	−5.9
3	−2.2	−8.1	5.8	−0.5	−0.2	−0.5	−1.4	−4.7
4	−2.0	−7.9	5.9	−0.5	−0.2	−0.5	−1.4	−4.5
5	−1.8	−17.4	15.6	−1.5	−2.6	−1.1	−1.5	−8.6
6	−2.1	−10.5	8.4	−0.9	−2.3	−0.5	−0.3	−6.2
7	−1.4	−9.8	8.5	−0.8	−2.2	−0.4	−0.3	−5.0
8	−1.7	−8.9	7.2	−0.5	−0.2	−0.5	−1.8	−4.7
9	−0.3	−6.4	6.2	−0.5	−1.2	−0.2	−0.4	−2.7
10	−0.5	−5.9	5.4	−0.4	−0.2	−0.2	−1.1	−2.5
11	0.3	−6.4	6.6	−0.3	−0.8	−0.2	−0.7	−1.7
12	0.3	−1.1	1.4	−0.2	0.0	0.0	−0.3	−0.2
13	−1.4	−12.4	10.9	−1.0	−2.9	−0.6	−0.2	−6.2
14	−0.7	−13.4	12.7	−1.3	−3.4	−0.7	−0.3	−6.4
w1	−1.9	−8.9	7.0	−0.4	−0.2	−0.5	−1.8	−4.9
w2	−1.7	−7.5	5.7	−0.4	−0.2	−0.5	−1.4	−4.2
w3	−1.8	−7.2	5.4	−0.4	−0.2	−0.5	−1.3	−4.1
w4	−2.1	−7.1	5.0	−0.3	−0.6	−0.3	−0.6	−3.8
w5	−2.0	−6.0	4.0	−0.3	−0.5	−0.2	−0.5	−3.4
w6	−2.0	−5.6	3.6	−0.3	−0.4	−0.2	−0.4	−3.3
w7	−1.8	−5.0	3.2	−0.1	−0.3	−0.2	−0.5	−2.8
w8	−0.5	−1.5	1.0	0.0	−0.2	0.0	−0.2	−1.1
w9	−1.7	−5.3	3.5	−0.2	−0.2	−0.1	−0.4	−2.7
w10	−1.2	−3.0	1.8	−0.1	−0.2	−0.1	−0.1	−1.8

basis sets (Tables 1, 2, S1 and S2) shows that all the components are affected by the use of the larger basis set; however, the BSSE energy is largely distributed into the charge-transfer term, which agrees with the previous studies [15, 35]. Moreover, for different software, different SCF convergence criteria and integration grid points are used, which leads to small deviations (Table S3) between the total energies given by the three programs. The subsequent discussion will be based on the results obtained with the 6-311++G(2d,2p) basis set for these water-containing dimers.

Table 1 shows the results from the CSOV decomposition on the 24 hydrogen-bonded dimers. It can be seen that all the components except the exchange repulsion term stabilize the dimers. The absolute value of the Coulomb term is the largest among all the negative components, which means it contributes the largest stabilization to the dimers. However, its stabilization effect is largely canceled out by the exchange repulsion term, which originates from the Pauli repulsion. As shown in Table 1, the polarization energies for monomer A and B are close to each other. In contrast, the charge-transfer energy from the hydrogen bond acceptor to the donor is much larger since the lone electron pairs of the acceptor are transferred to the donor. Using dimer 3 as an example, the charge-transfer energy

from formamide to water is much smaller than the one from water to formamide. This is because the electron of the oxygen atom of water acts as the hydrogen bond donor to formamide. This indicates that the charge transfer helps the formation of hydrogen bonds and stabilizes the dimers. This is consistent with the role of the charge transfer from the lone pair of the proton acceptor to the empty anti-bonding orbital of the proton donor in lowering the barrier for proton transfer [46, 47]. The importance of the charge-transfer contribution in intermolecular interactions has also been pointed out in the framework of the CSOV analysis assists weight increases when including dynamic correlation with DFT [35].

When scrutinizing the components from CSOV, they are highly related to the chemical properties of the dimers. Generally speaking, the dimers that exhibit more negative total interactions for the dimers show NCI surfaces that are deeper blue (see Fig. 1). The deeper blue surfaces indicate stronger attractive interactions. For example, dimer 1 (formamide–water) and 5 (N-methylformamide–water), which have two dark blue surfaces are most strongly bound. In contrast, dimer 12 (methane–water), which only possess a small green surface indicating weak interaction, is least bound. All CSOV components for this dimer are small, especially the Coulomb term. This is likely because

Table 2 DFT steric analysis on water-containing dimers (unit: kcal/mol; B3LYP/6-311++G(2d,2p))

Dimers	ΔT_s	ΔE_e	ΔE_{xc}	ΔE_x	ΔE_c	ΔE_s	ΔE_{Pauli}	ΔE_q	E_{tot}
1	36.1	−27.0	−17.5	−12.9	−4.6	−171.4	207.5	190.0	−8.4
2	19.6	−14.1	−11.3	−8.1	−3.2	−120.9	140.5	129.2	−5.9
3	14.6	−11.0	−8.3	−6.0	−2.3	−90.6	105.2	96.9	−4.7
4	13.0	−9.7	−7.9	−5.6	−2.3	−91.9	104.9	97.1	−4.5
5	37.2	−28.0	−17.9	−13.2	−4.7	−177.6	214.8	196.9	−8.7
6	19.9	−14.8	−11.4	−8.2	−3.2	−122.5	142.4	131.0	−6.3
7	19.8	−14.7	−10.1	−7.3	−2.8	−112.2	132.0	121.9	−5.1
8	10.8	−7.4	−8.1	−5.6	−2.5	−101.5	112.3	104.2	−4.7
9	7.2	−4.8	−4.7	−3.3	−1.5	−62.2	69.4	64.6	−2.3
10	12.6	−9.6	−5.4	−3.6	−1.8	−69.0	81.6	76.1	−2.5
11	15.3	−10.8	−6.4	−4.8	−1.6	−60.6	75.9	69.4	−2.0
12	4.1	−2.4	−1.9	−0.9	−1.0	−34.3	38.4	36.4	−0.2
13	21.2	−16.3	−11.2	−8.3	−2.9	−107.2	128.4	117.2	−6.3
14	27.4	−21.3	−12.7	−9.3	−3.4	−124.3	151.7	139.1	−6.5
w1	13.6	−10.0	−8.5	−6.0	−2.4	−98.5	112.1	103.6	−4.9
w2	10.9	−7.4	−7.6	−5.4	−2.3	−93.4	104.3	96.6	−4.2
w3	10.2	−6.7	−7.6	−5.3	−2.2	−93.5	103.7	96.1	−4.1
w4	12.7	−9.8	−6.8	−4.3	−2.5	−94.6	107.3	100.6	−3.8
w5	11.1	−8.1	−6.4	−4.0	−2.4	−93.1	104.2	97.8	−3.4
w6	10.4	−7.4	−6.3	−4.0	−2.4	−93.0	103.4	97.1	−3.3
w7	6.9	−5.3	−4.4	−2.5	−2.0	−74.7	81.6	77.2	−2.8
w8	0.5	−0.4	−1.2	−0.3	−0.9	−35.0	35.5	34.3	−1.1
w9	5.3	−3.4	−4.7	−2.8	−1.9	−76.0	81.3	76.7	−2.7
w10	1.9	−0.4	−3.2	−1.9	−1.3	−56.3	58.2	54.9	−1.8

methane is a nonpolar molecule. Comparing dimer 13 (ammonia–water) and 14 (methylamine–water), the addition of the methyl group, an electron-donating group, increases the charge transfer from the nitrogen to the hydrogen of the water and therefore makes the dimer more strongly bound. This type of stabilization effects from the methyl group can also be found by comparing dimer 7 (methanol–water) and the water dimers. However, if an electron-donating group is added to the hydrogen bond acceptor, it will decrease the charge-transfer ability, which can be verified by the charge-transfer energy from methanol to water for dimer 7 is more negative than the one from water to methanol for dimer 8 (methanol–water). In addition to the relatively low attractions between the monomers, the repulsions between the oxygen of the water molecule and the carbon atom of the other monomer also lead to relatively high E_{tot}. dimer 9 (fluomethane–water), 10 (dichloromethane–water), and 11 (difluoromethane–water) are the examples.

The DFTs–EDA results in Table 2 show that the electrostatic (E_e) and steric (E_s) interactions for the dimers are lower than the sum of these components from its two composite monomers. The stabilization effect is dominated by the change of E_s. In contrast, E_q, which

includes E_{xc} and E_{Pauli}, increases when forming the dimers. As the value of ΔE_{xc} is negative, ΔE_{Pauli} contributes mostly to the destabilization effect. Regarding the traditional partitions, ΔT_s, which also contains ΔE_{Pauli}, is the only component destabilizing the dimers. The formation of dimers is favored by the steric, electrostatic, as well as correlation interactions, while it is not favored by the quantum effects, which mainly come from the Pauli Exclusion Principle. This finding agrees well with the CSOV analysis with regarding to the destabilization effects arising from the Pauli repulsion. For the traditional DFT partition, ΔE_e has the largest stabilization effect. For the DFT steric analysis, the stabilization effect is dominated by ΔE_s. The plots of the total interaction energy versus E_{Coul}, ΔE_e, and ΔE_s, respectively, are shown in Fig. 2. Linear relationships can be found between these dominant components for each partition method with total interaction energy, and the linear relationships between the DFTs–EDA components and the total energy are conserved for water clusters [48]. Out of these three, E_{Coul} from CSOV and ΔE_s from DFT steric analysis have better linear relationships ($R^2 > 0.93$) with E_{tot}. The former suggests the importance of the stabilization effects from the
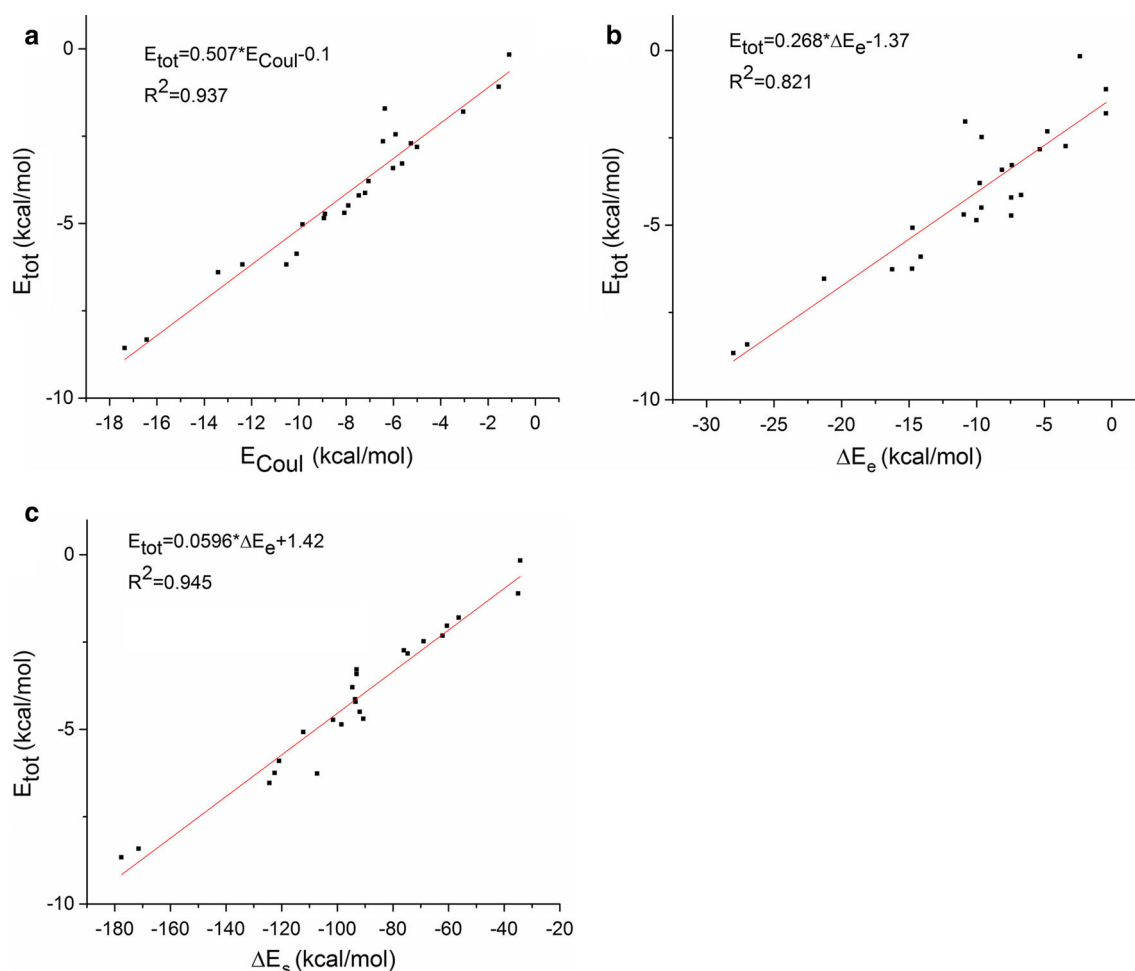
Fig. 2 Linear fitting of E_e versus E_{Coul} (**a**), ΔE_e (**b**), and ΔE_s(**c**)

electrostatic interaction in forming hydrogen bonds, and the latter indicates the critical role of the spatial rearrangement of the electron in the formation of these hydrogen-bonded dimers, which is represented by ΔE_s.

In addition, previous studies have shown that there is a direct relationship between the electron density at the intermolecular bond critical points and the total intermolecular interaction [49]. We performed Bader's QTAIM analysis on the ten water dimers to determine a possible relationship between the electron density at the intermolecular bond critical point (BCPs) and ΔE_s. We have considered only the water dimers in this case since they only have one intermolecular BCP. To confirm our results, a good linear relationship between the intermolecular BCP's electron density (ρ_{BCP}) and the total interaction energy can be seen in Fig. 3a. The relationship can be explained by that stronger hydrogen-bonding dimers have more charge transfer or (and) polarization and hence more electron mixing. As a result, the electron density at the critical point is larger. In addition, the definition of the DFT steric energy (Eq. 3) tells us its

value is determined only by the electron density and its gradient. Is there a relationship between ΔE_s and the electron density at intermolecular BCPs where the electron density gradient is zero? The plot in Fig. 3b indicates there is indeed a good linear relationship ($R^2 = 0.904$) between ΔE_s and $1/\rho_{BCP}$. The slope is positive, which means the dimer with a large ρ_{BCP} has smaller stabilization from ΔE_s. As monomers approach each other to form a dimer, the electron density and its gradient in space, especially around the area where the hydrogen bond forms, will be rearranged accordingly. As an example, Fig. 4 compares the plots of the electron gradient versus the electron density for the water monomer (Fig. 4a) and the canonical water dimer (w1, Fig. 4b). It can be qualitatively seen that the electron density change mostly comes from the peak that belongs to the hydrogen bonding. This plot is similar to the plot between the reduced density gradient and the product of the sign of λ2 and the electron density obtained by NCI [36, 43]. As mentioned before, stronger hydrogen-bonding dimers have more mixing. The more relaxed the electron distribution
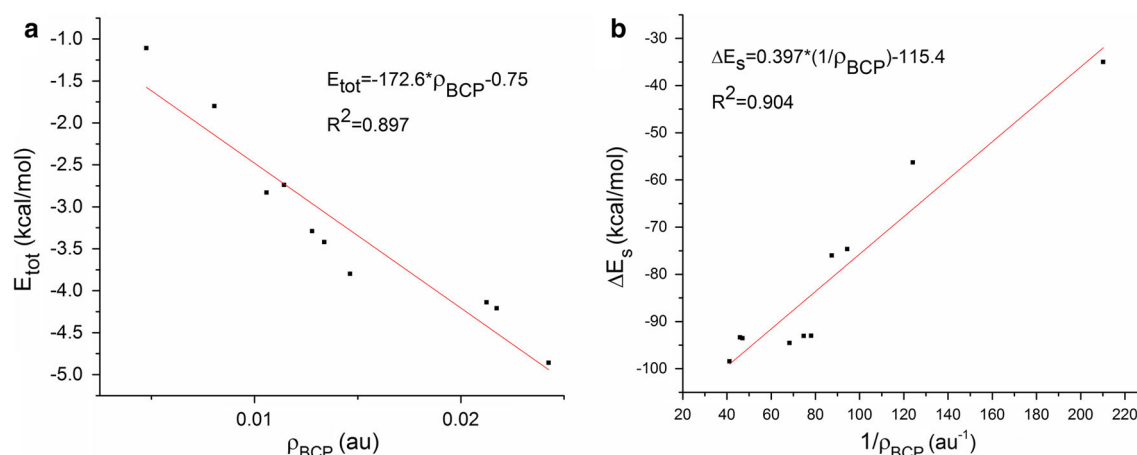
Fig. 3 Linear fitting of E_{tot} versus ρ_{BCP} (**a**) and ΔE_s versus $1/\rho_{BCP}$ (**b**) for water dimers
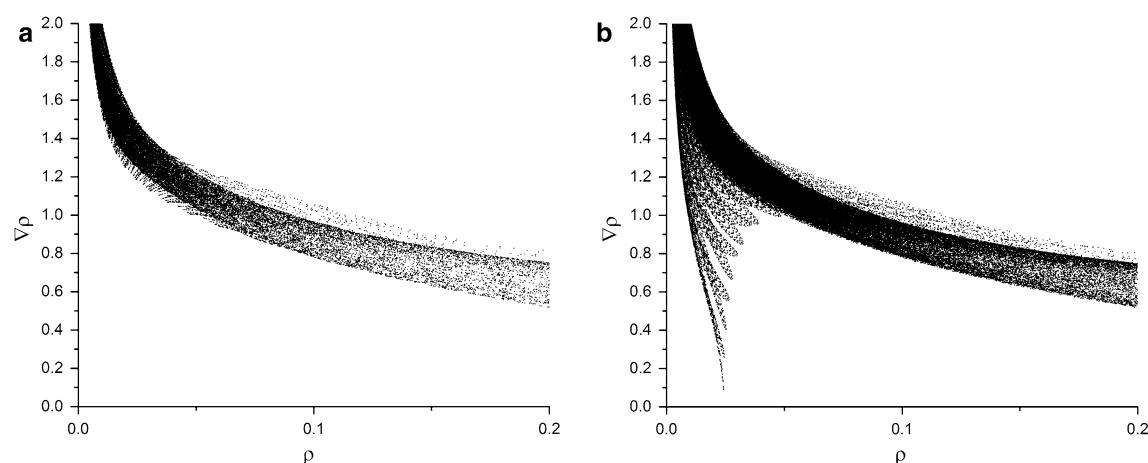

Fig. 4 Plots of $\nabla\rho$ versus ρ for dimer *w1*: **a** monomer; **b** dimer (Cutoff for $\nabla\rho$ and ρ is 2 and 0.2, respectively, to show the intermolecular points)

is, the gradient becomes smaller, and the electron density around the critical points is larger. According to Eq. 3, both make the steric energy smaller. Therefore, stronger hydrogen-bonding dimers have lower steric energy. Similarly, for the water dimers, the change of DFT steric energy for forming dimers may be also mainly due to the interactions arising from the hydrogen-bonding region, which helps explain why ΔE_s correlates with the electron density at the intermolecular BCPs.

To gain a further understanding of the components of the DFT steric analysis, we have compared the individual components from this decomposition to individual terms obtained with CSOV. For the electrostatic interactions, a good linear relationship is observed (see Fig. 5a) even though the magnitudes of the values differ between these two methods. The Coulomb interaction from CSOV is less negative than that from steric analysis because CSOV utilizes unperturbed orbitals of monomers, while steric analysis uses completely relaxed orbitals of dimers. Since charge transfer and polarization are due to the relaxation of

the orbitals, the relationship between $E_{Coul} + E_{CT} + E_{Pol}$ and ΔE_e is plotted in Fig. 5b. It is shown that their linear relationship is slightly better, which suggests charge transfer and polarization may include some electrostatic effects from the relaxation of the orbitals. The $E_{Exch-Rep}$ from CSOV, which is related to the Pauli Exclusion Principle, is comparable to ΔE_x and ΔE_{Pauli}. It can be seen that the $E_{Exch-Rep}$ interaction from CSOV is positive compared with ΔE_x from DFTs–EDA, which is negative (see Table 2). This suggests that the Pauli repulsion from CSOV is so positive that it cancels the stabilization effect from the exchange compared with the stabilization effect from the correlation energy. It should be mentioned here that the exchange from DFTs–EDA, which reflects the energy change when switching the spatial positions of the two electrons interchanged, does not include repulsion effects. The linear fitting of $E_{Exch-Rep}$ from CSOV versus E_x and E_{Pauli} is shown in Fig. 6a, b. Figure 6c shows the linear relationship between $E_{Pol} + E_{CT}$ and the steric energy. For the uniform electron gas, because the gradient

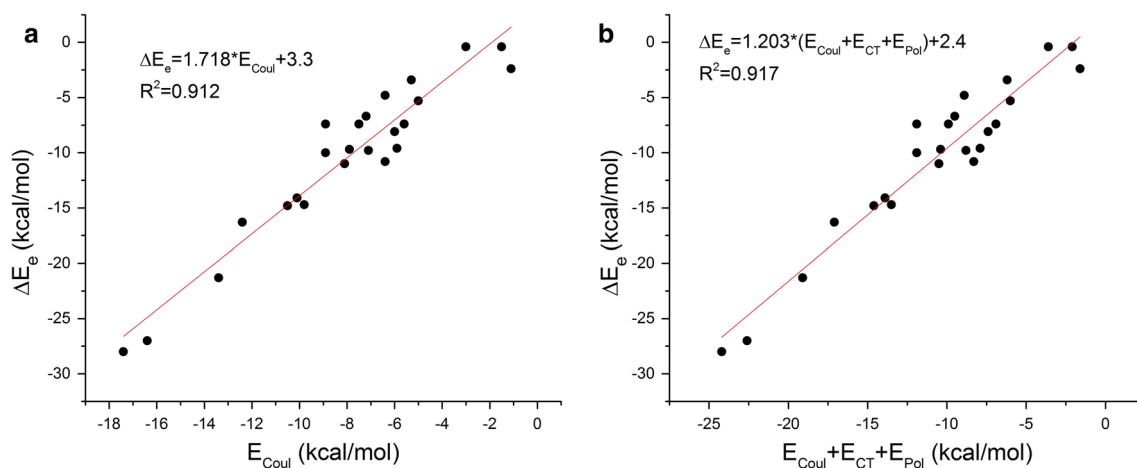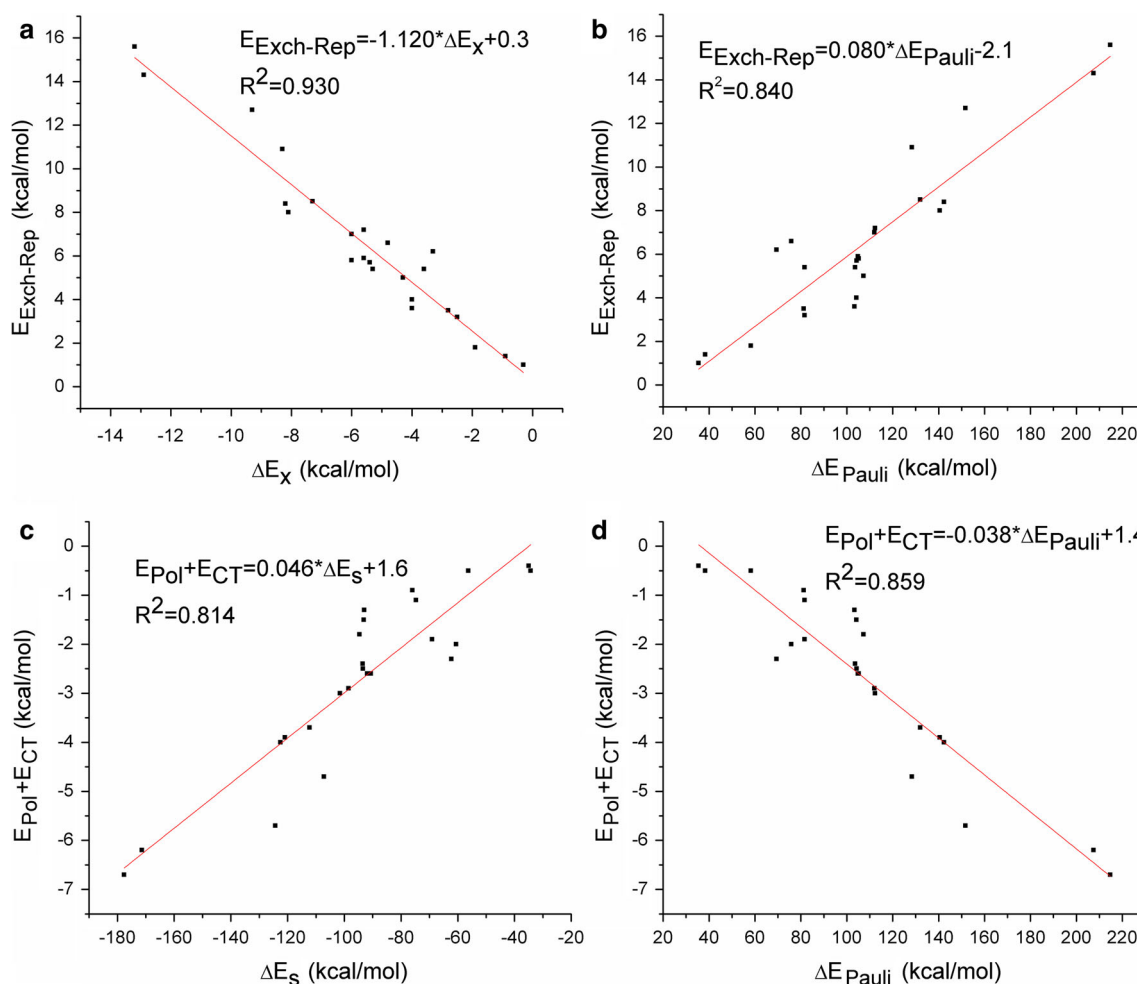**Fig. 5** Linear fitting of ΔE_e versus E_{Coul} (**a**) and $E_{Coul} + E_{CT} + E_{Pol}$ (**b**) for water dimers

Fig. 6 Linear fitting of $E_{Exch-Rep}$ versus ΔE_X (**a**), $E_{Exch-Rep}$ versus ΔE_S (**b**), $E_{Pol} + E_{CT}$ versus ΔE_S (**c**), and $E_{Pol} + E_{CT}$ versus ΔE_{Pauli} (**d**) for water dimers

of the electron density is zero, the steric energy is zero according to Eq. 3. In this regard, the steric energy reflects the change of the electron density going from the ideal

noninteracting electron gas to the molecular environment. For CSOV, as described in the previous section, the polarization and the charge-transfer components describe

Table 3 CSOV decomposition on DNA base pair (unit:kcal/mol; B3LYP/6-31G(d))

Dimers	E_{FC}	E_{Coul}	$E_{Exch-Rep}$	E_{PolA}	$E_{CT(A\rightarrow B)}$	E_{PolB}	$E_{CT(B\rightarrow A)}$	E_{tot}
A–T	−1.4	−23.9	22.6	−2.6	−6.7	−1.9	−5.1	−18.1
C–G	−7.1	−28.1	21.0	−3.8	−7.4	−2.6	−4.7	−25.5

Table 4 DFT steric analysis on DNA base pair (unit:kcal/mol; B3LYP/6-31G(d))

Dimers	ΔT_s	ΔE_e	ΔE_{xc}	ΔE_x	ΔE_c	ΔE_s	ΔE_q	E_{tot}
A–T	50.5	−51.3	−17.5	−11.0	−6.4	−250.7	283.7	−18.3
C–G	41.6	−48.6	−19.1	−11.8	−7.3	−301.8	324.2	−26.2
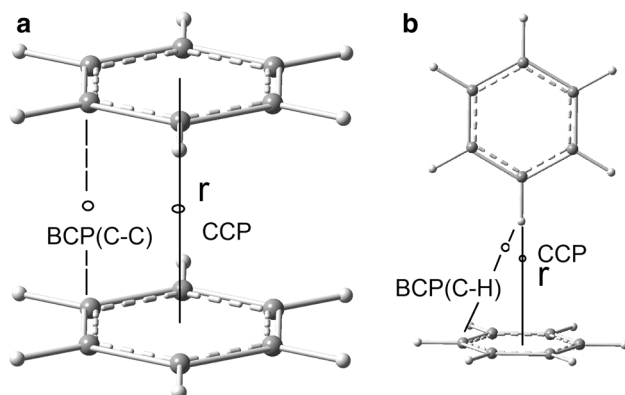
Fig. 7 Structures of benzene dimers (*r* represents the distance). For **a**, it is the distance between the centers of two monomers. For **b**, it is the distance between one hydrogen atom of the upper benzene and the center of the other monomer. *Black circles* are critical points for AIM. For BCPs, only one is shown for illustration (BCP stands for bond critical point, and CCP is cage critical point)

the change in the orbitals (occupied and virtual) of one monomer due to the presence of the perturbing field produced by the other monomer. The effects of these two energy components are also reflected on the change of the electron density and its gradient in the dimers. From the perspective of chemical meaning, the steric energy qualitatively represents the steric effect, which represents the effects from the spatial redistribution of the electron density when atoms or molecules are brought together [14, 50]. Thus, the polarization and charge transfer from CSOV may capture the steric effect to some extent as well. As ΔE_{Pauli} represents the effects that Pauli's exclusion principle take on the kinetic energy, and Pauli exclusion also takes part in the relaxation of the orbitals for calculation, the linear relationship between $E_{Pol} + E_{CT}$ and ΔE_{Pauli} has been fitted in Fig. 6d. $E_{Pol} + E_{CT}$ and the steric energy are negative, while ΔE_{Pauli} is positive, which suggests that the steric energy contributes more to the $E_{Pol} + E_{CT}$ than ΔE_{Pauli}.

Two DNA base pairs (Figure S1), guanine-cytosine and adenine–thymine paired in the canonical Watson–Crick conformation, have also been studied. Because of the

limitation on computation time needed by CSOV, the smaller basis set 6-31G(d) was adopted for these two dimers and for the benzene dimers discussed in the following subsection. The results for CSOV and DFT steric analysis are summarized in Tables 3 and 4, respectively. As shown in Table 3, for multiple hydrogen-bonding dimers, the sum of the polarization and charge-transfer energy increases and becomes comparable to the Coulomb interaction. Compared with the previous result [35] with a larger basis set, this increase in charge transfer is not only because of the increasing number of hydrogen bonds, but also due to the BSSE effect on the charge-transfer component due to the small basis set employed. It can be seen from Table 4 that the pair with lower total interaction energy has a lower ΔE_s value, which is consistent with the hydrogen-bonded dimers above. In addition, after the mixing of the orbitals of the monomers, ΔE_e given by steric analysis for A–T is more negative than C–G, while the trend is opposite with respect to $\Delta E_{Coulomb}$ from CSOV.

3.2 Benzene dimers

Two types of benzene dimers (Fig. 7), sandwich and T-shaped, calculated at varying intermolecular distances have been investigated. These two types of benzene dimers have been studied extensively by high-level methods such as MP2, CCSD(T), SAPT–DFT in order to obtain accurate intermolecular interaction energies [51–60]. It is known that traditional DFT methods like B3LYP fail to predict accurate interaction energies for these benzene dimers because of the lack of dispersion term. However, in most cases for DFT, the dispersion may be treated by empirical corrections and it can be separated when performing EDA [18], which provides us the chance to do EDA analysis on the dimers using B3LYP without dispersion term.

Regarding the sandwich benzene dimer, because of the missing dispersion term, which is one of the main sources to introduce the stabilization effects, the total energies are positive at all distances. It has been proposed that besides the dispersion term, electrostatic interaction, and steric repulsion govern the total interaction energy as well [52]. As

Table 5 CSOV decomposition on sandwich benzene dimer (unit:kcal/mol; B3LYP/6-31G(d))

r(Å)	E_{FC}	E_{Coul}	$E_{Exch-Rep}$	E_{PolA}	$E_{CT(A \to B)}$	E_{PolB}	$E_{CT(B \to A)}$	E_{tot}
3.4	7.7	0.2	7.4	−0.1	−0.6	−0.1	−0.6	6.2
3.5	6.1	0.6	5.4	−0.1	−0.6	−0.1	−0.6	4.6
3.6	4.8	0.8	4.0	−0.1	−0.6	−0.1	−0.6	3.5
3.7	3.9	0.9	3.0	−0.1	−0.6	−0.1	−0.6	2.6
3.8	3.2	1.0	2.2	−0.1	−0.6	−0.1	−0.6	2.0
3.9	2.7	1.0	1.7	−0.1	−0.5	0.0	−0.5	1.6
4.0	2.3	0.9	1.4	0.0	−0.5	0.0	−0.5	1.3
4.1	2.0	0.9	1.1	0.0	−0.4	0.0	−0.4	1.1
4.2	1.7	0.9	0.9	0.0	−0.3	0.0	−0.3	1.0
4.3	1.4	0.8	0.6	0.0	−0.3	0.0	−0.3	0.8
4.4	1.2	0.8	0.5	0.0	−0.2	0.0	−0.2	0.8
5.0	0.7	0.5	0.2	0.0	0.0	0.0	0.0	0.6
5.5	0.4	0.4	0.0	0.0	0.0	0.0	0.0	0.4
6.0	0.3	0.3	0.0	0.0	0.0	0.0	0.0	0.3
8.0	0.1	0.1	0.0	0.0	0.0	0.0	0.0	0.1
9.0	0.1	0.1	0.0	0.0	0.0	0.0	0.0	0.0
10.0	0.0	0.0	0.0	0.0	0.0	0.0	0.0	0.0

Table 6 DFT steric analysis on sandwich benzene dimer (unit:kcal/mol; B3LYP/6-31G(d))

r(Å)	ΔT_s	ΔE_e	ΔE_{xc}	ΔE_x	ΔE_c	ΔE_s	ΔE_q	E_{tot}
3.4	−13.7	23.8	−4.0	−0.1	−4.0	−126.9	109.2	6.1
3.5	−7.3	15.0	−3.1	0.1	−3.2	−108.6	98.2	4.5
3.6	−2.7	8.5	−2.4	0.2	−2.6	−92.6	87.5	3.4
3.7	0.6	3.8	−1.8	0.3	−2.1	−78.6	77.4	2.6
3.8	2.8	0.6	−1.4	0.3	−1.7	−66.4	67.8	2.0
3.9	4.2	−1.6	−1.0	0.3	−1.3	−55.8	58.9	1.6
4.0	4.9	−2.9	−0.7	0.3	−1.0	−46.5	50.8	1.3
4.1	5.2	−3.7	−0.5	0.3	−0.8	−38.7	43.4	1.1
4.2	5.2	−4.0	−0.3	0.3	−0.6	−31.9	36.9	1.0
4.3	5.0	−4.0	−0.2	0.2	−0.4	−26.2	31.1	0.9
4.4	4.7	−3.8	−0.1	0.2	−0.3	−21.4	26.0	0.8
5.0	2.8	−2.3	0.1	0.1	0.0	−5.5	8.4	0.6
5.5	2.0	−1.7	0.1	0.1	0.1	−1.4	3.4	0.4
6.0	1.5	−1.3	0.1	0.0	0.0	−0.2	1.7	0.3
8.0	0.5	−0.4	0.0	0.0	0.0	0.1	0.4	0.1
9.0	0.3	−0.3	0.0	0.0	0.0	0.0	0.3	0.1
10.0	0.2	−0.2	0.0	0.0	0.0	0.0	0.2	0.0

shown by the CSOV results in Table 5, the destabilization effects are mainly contributed by the exchange repulsion term. It decreases dramatically with the increasing of the distance. The Coulomb term also destabilizes the dimers. It first increases and then decreases with the increasing of the distance. Compared with the charge-transfer term, the polarization energy is smaller. Both of them stabilize the dimers. On the other hand, in the case of the DFT steric results shown in Table 6, the electrostatic term (ΔE_e) is much

larger than ($E_{Coulomb}$) from the CSOV analysis at short distances and then decreases to a negative value at long distances. When it comes to ΔE_s, instead of positive values that are indicative of the destabilization effects, the values of ΔE_s are negative. As shown in the definition, the DFT steric term excludes the effects from the Pauli Exclusion Principle and should be indicative of pure spatial effects from the rearrangements of the electrons. The so-called steric repulsion for the sandwich benzene dimer should refer to the Pauli repulsion, which is included in ΔE_q and similar to the proposed concept called steric strain [31].

We have also calculated intermolecular BCPs and their electron density for these dimers. Two types of intermolecular critical points (CP), BCPs and Cage Critical Points (CCP), are depicted in Fig. 7. It can be seen that these two types of points have a good linear relationship with each other as shown in Fig. 8. It can be seen that in contrast to the water dimers discussed above, $\rho_{BCP(C-C)}$ and E_{tot} do not show a linear relationship. However, $\rho_{BCP(C-C)}$ correlates linearly with ΔE_s with a negative slope. This is consistent with the decreasing trend in ΔE_s as the electron density increases at intermolecular BCPs, similar to the effect observed in the water dimers above.

Since dispersion is not the main contribution to the total interaction energy for the T-shaped benzene dimer, the values of the total interaction energy obtained by B3LYP (see Tables 7, 8) are negative and closer to the results from the high-level methods [51]. Within the separation distances we studied, the results from CSOV show that Coulomb interaction stabilizes the dimer, which is consistent with the previous SAPT–DFT result [55]. However, after the mixing of the orbitals of the dimers, the energy
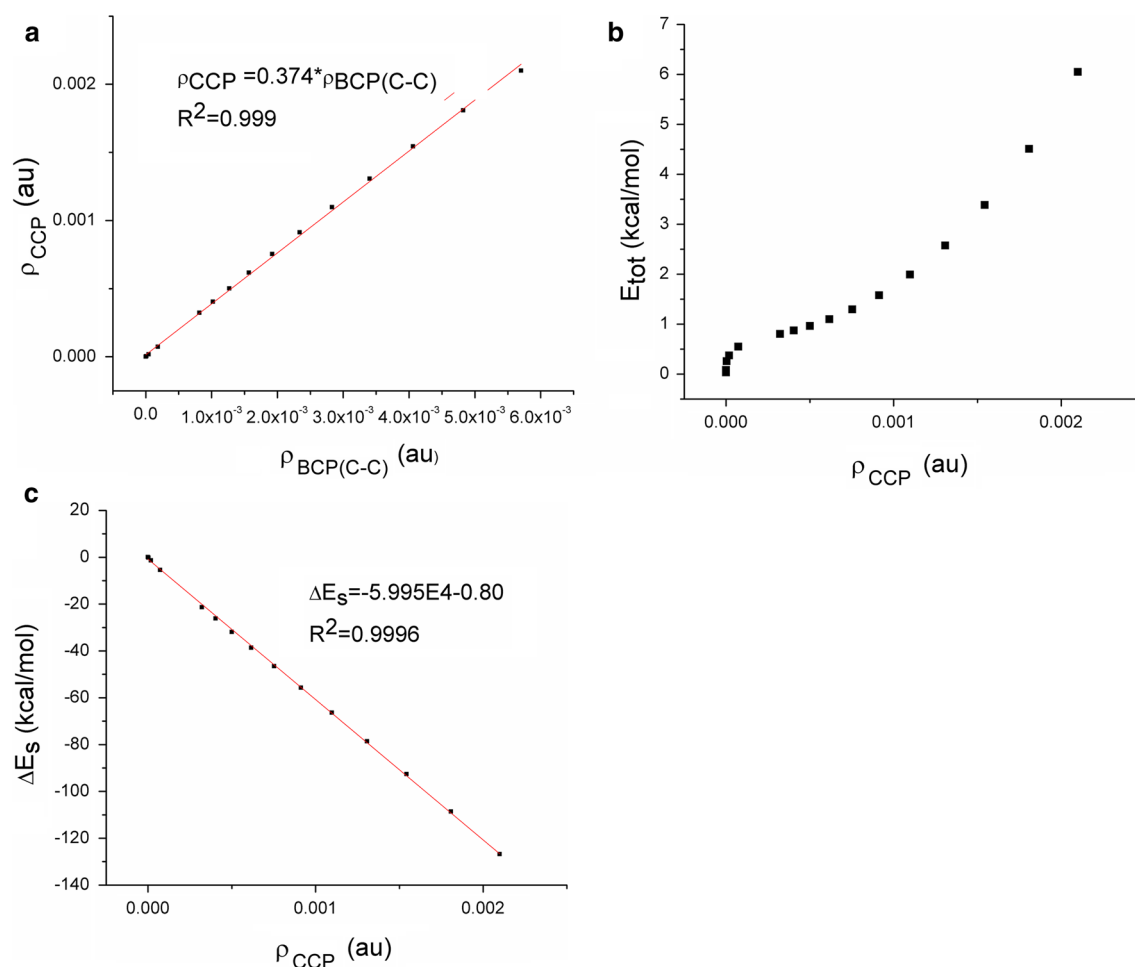
Fig. 8 **a** Linear fitting of ρ_{CCP} versus $\rho_{BCP(C–C)}$. **b** *Plot* of E_{tot} versus ρ_{CCP}. **c** Linear fitting of ΔE_s versus ρ_{CCP} for the benzene dimer in the sandwich conformation

Table 7 CSOV decomposition on T-shaped benzene dimers with B3LYP/6-31G(d) (unit: kcal/mol; the upper benzene is denoted as A)

$r(\text{Å})$	E_{FC}	E_{Coul}	$E_{Exch–Rep}$	E_{PolA}	$E_{CT(A \to B)}$	E_{PolB}	$E_{CT(B \to A)}$	E_{tot}
3.0	0.2	−0.5	0.7	−0.1	−0.1	0.0	−0.7	−0.6
3.2	0.2	−0.4	0.5	−0.1	−0.1	0.0	−0.5	−0.5
3.4	−0.1	−0.3	0.2	−0.1	0.0	0.0	−0.4	−0.5
3.6	−0.1	−0.2	0.2	0.0	0.0	0.0	−0.3	−0.5
3.8	0.0	−0.2	0.2	0.0	0.0	0.0	−0.2	−0.3
4.0	0.0	−0.2	0.2	0.0	0.0	0.0	−0.2	−0.2

becomes positive and destabilizes the dimer, as indicated by the results from DFT steric analysis. Both methods indicate the destabilization effects arise from the exchange term. As shown by the results from CSOV, the charge transfer from the bottom benzene to the upper benzene, mainly π electron transferred to the empty orbital of the hydrogen atom, is comparable to the Coulomb term. The plots of E_{tot} and ΔE_s versus ρ_{CCP} are shown in Fig. 9. It is observed that ΔE decreases with the increasing of ρ_{CCP}, which correlates linearly with ΔE_s.

Table 8 DFT Steric Analysis on T-shaped benzene dimers with B3LYP/6-31G(d) (kcal/mol)

$r(\text{Å})$	ΔT_s	ΔE_e	ΔE_{xc}	ΔE_x	ΔE_c	ΔE_s	ΔE_q	E_{tot}
3.0	−2.2	1.5	0.0	0.8	−0.8	−29.9	27.7	−0.7
3.2	−1.4	0.6	0.3	0.8	−0.5	−21.4	20.2	−0.6
3.4	−1.0	0.2	0.3	0.6	−0.3	−15.0	14.4	−0.5
3.6	−0.7	0.1	0.3	0.5	−0.2	−10.4	9.9	−0.4
3.8	−0.6	0.1	0.2	0.3	−0.1	−7.1	6.6	−0.3
4.0	−0.5	0.2	0.0	0.1	−0.1	−4.7	4.2	−0.3
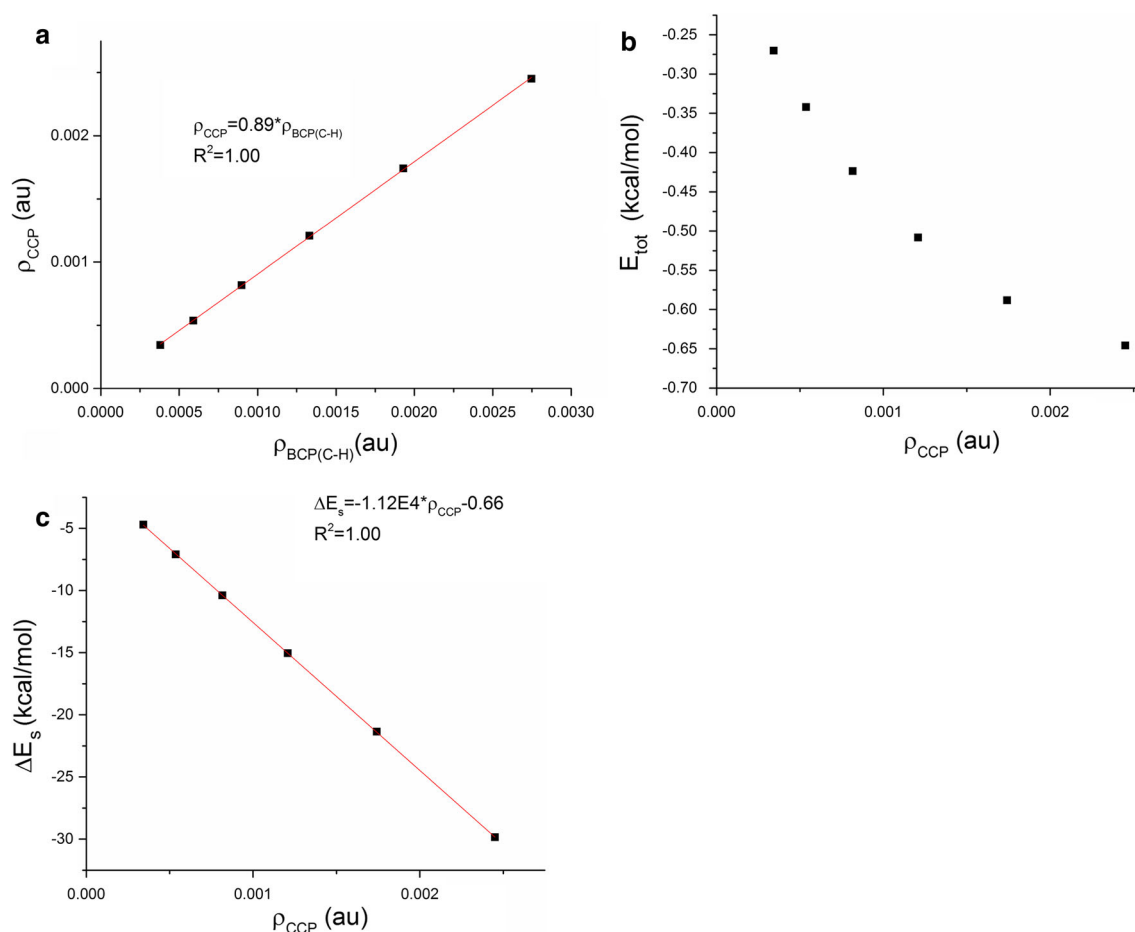
Fig. 9 **a** Linear fitting of ρ_{CCP} versus $\rho_{BCP(C–H)}$. **b** *Plot* of E_{tot} versus ρ_{CCP}. **c** Linear fitting of ΔE_s versus ρ_{CCP} for the T-shaped benzene dimer

4 Conclusions

Herein, we have applied density functional steric analysis, a new energy decomposition method, combined with the CSOV and QTAIM to investigate the components that contribute to the total interaction for dimers from a different perspective. One can gain more understandings of the origins of the formation of dimers by combining these two analyses. It has been shown that there is a good linear relationship between the change of DFT steric energy and the total interaction energy for hydrogen-bonding dimers. In addition, comparisons between components of CSOV and DFT steric energy decomposition show the effects of the relaxation of the orbitals of monomers and the linear relationship between the polarization and charge transfer from CSOV and the steric and Pauli energy from DFT steric analysis. In combination with QTAIM analysis, it has been found that the change of DFT steric energy directly correlates with the electron density in the critical points. This suggests the steric energy is indicative of the energy change arising from the spatial distribution of the electron density and also helps explain the connection between the change of DFT steric energy and the total interaction energy. This new decomposition method provides a way to quantify the spatial effects on the electron density change during the formation of dimers.

5 Supporting information

Results of CSOV and density functional steric analysis on water-containing dimers with 6-31G(d) basis set, the deviation table, the BSSE table, the structures of DNA base pair, the electron density at BCPs for water dimers and at BCPs and CCPs for benzene dimers are provided in supporting information.

References

1. Hirschfelder JO (1967) Chem Phys Lett 1:363–368
2. Murrell JN, Shaw G (1967) J Chem Phys 46:1768–1772
3. Kitaura K, Morokuma K (1976) Int J Quantum Chem 10:325–340
4. Ziegler T, Rauk A (1979) Inorg Chem 18:1558–1565

5. Bagus PS, Hermann K, Bauschlicher JCW (1984) J Chem Phys 80:4378–4386
6. Stevens WJ, Fink WH (1987) Chem Phys Lett 139:15–22
7. Glendening ED, Streitwieser A (1994) J Chem Phys 100:2900–2909
8. Jeziorski B, Moszynski R, Szalewicz K (1994) Chem Rev 94:1887–1930
9. Chen W, Gordon MS (1996) J Phys Chem 100:14316–14328
10. Mo Y, Gao J, Peyerimhoff SD (2000) J Chem Phys 112:5530–5538
11. Mayer I (2003) Chem Phys Lett 382:265–269
12. Hesselmann A, Jansen G, Schutz M (2005) J Chem Phys 122:014103–014117
13. Khaliullin RZ, Cobar EA, Lochan RC, Bell AT, Head-Gordon M (2007) J Phys Chem A 111:8753–8765
14. Liu S (2007) J Chem Phys 126:244103–244105
15. Reinhardt P, Piquemal J-P, Savin A (2008) J Chem Theory Comput 4:2020–2029
16. Cisneros GA, Darden TA, Gresh N, Reinhardt P, Parisel O, Pilmé J, Piquemal J-P (2009) Design of next generation polarizable force fields from ab initio computations: beyond point charges. Multi-scale quantum models for biocatalysis: modern techniques and applications, for the book series: challenges and advances in computational chemistry and physics. Springer, London
17. Su P, Li H (2009) J Chem Phys 131:014102–014115
18. Wu Q, Ayers PW, Zhang Y (2009) J Chem Phys 131:164112–164118
19. Steinmann SN, Corminboeuf C, Wu W, Mo Y (2011) J Phys Chem A 115:5467–5477
20. Azar RJ, Head-Gordon M (2012) J Chem Phys 136:024103–024108
21. Szczesniak MM, Chalasinski G, Cybulski SM (1992) J Chem Phys 96:463–469
22. Khaliullin RZ, Bell AT, Head-Gordon M (2009) Chem Eur J 15:851–855
23. Liu S, Govind N (2008) J Phys Chem A 112:6690–6699
24. Huang Y, Zhong A-G, Yang Q, Liu S (2011) J Chem Phys 134:084103–084109
25. Liu S, Hu H, Pedersen LG (2010) J Phys Chem A 114:5913–5918
26. Bader RFW (1985) Acc Chem Res 18:9–15
27. Weizsacker CFV (1935) Z Phys A Hadrons Nucl 96:431
28. Rong C, Lu T, Liu S (2014) J Chem Phys 140:024109
29. Badenhoop JK, Weinhold F (1997) J Chem Phys 107:5406–5421
30. Nagy Á (2007) Chem Phys Lett 449:212–215
31. Pinter B, Fievez T, Bickelhaupt FM, Geerlings P, De Proft F (2012) Phys Chem Chem Phys 14:9846–9854
32. Bagus PS, Illas F (1992) J Chem Phys 96:8962–8970
33. Neyman KM, Ruzankin SP, Rösch N (1995) Chem Phys Lett 246:546–554
34. Márquez AM, López N, García-Hernández M, Illas F (1999) Surf Sci 442:463–476
35. Piquemal J-P, Marquez A, Parisel O, Giessner-Prettre C (2005) J Comput Chem 26:1052–1062
36. Johnson ER, Keinan S, Mori-Sánchez P, Contreras-García J, Cohen AJ, Yang W (2010) J Am Chem Soc 132:6498–6506
37. Lee C, Yang W, Parr RG (1988) Phys Rev B 37:785–789
38. Becke AD (1993) J Chem Phys 98:5648–5652
39. Frisch MJ, Trucks GW, Schlegel HB, Scuseria GE, Robb MA, Cheeseman JR, Scalmani G, Barone V, Mennucci B, Petersson GA, Nakatsuji H, Caricato M, Li X, Hratchian HP, Izmaylov AF, Bloino J, Zheng G, Sonnenberg JL, Hada M, Ehara M, Toyota K, Fukuda R, Hasegawa J, Ishida M, Nakajima T, Honda Y, Kitao O, Nakai H, Vreven T, Montgomery JA, Peralta JE, Ogliaro F, Bearpark M, Heyd JJ, Brothers E, Kudin KN, Staroverov VN, Kobayashi R, Normand J, Raghavachari K, Rendell A, Burant JC, Iyengar SS, Tomasi J, Cossi M, Rega N, Millam JM, Klene M, Knox JE, Cross JB, Bakken V, Adamo C, Jaramillo J, Gomperts R, Stratmann RE, Yazyev O, Austin AJ, Cammi R, Pomelli C, Ochterski JW, Martin RL, Morokuma K, Zakrzewski VG, Voth GA, Salvador P, Dannenberg JJ, Dapprich S, Daniels AD, Farkas, Foresman JB, Ortiz JV, Cioslowski J, Fox DJ (2009) Gaussian 09, Revision B.01. Gaussian, Inc., Wallingford
40. Boys SF, Bernardi F (1970) Mol Phys 19:553–566
41. Dupuis M, Marquez A, Davidson ER (1999) HONDO 95.3. Quantum Chemistry Program Exchange (QCPE), Bloomington
42. Valiev M, Bylaska EJ, Govind N, Kowalski K, Straatsma TP, Van Dam HJJ, Wang D, Nieplocha J, Apra E, Windus TL, de Jong WA (2010) Comput Phys Commun 181:1477–1489
43. Contreras-García J, Johnson ER, Keinan S, Chaudret R, Piquemal J-P, Beratan DN, Yang W (2011) J Chem Theory Comput 7:625–632
44. Humphrey W, Dalke A, Schulten K (1996) J Mol Graph 14:33–38
45. Balabin RM (2008) J Chem Phys 129:164101–164105
46. Saritha B, Durga Prasad M (2012) J Chem Sci 124:209–214
47. Saritha B, Durga Prasad M (2011) J Phys Chem A 115:2802–2810
48. Wang Y, Zhao D, Rong C, Liu S (2013) Acta Phys Chim Sin 29:2173
49. Parthasarathi R, Subramanian V, Sathyamurthy N (2006) J Phys Chem A 110:3349–3351
50. Ess DH, Liu S, De Proft F (2010) J Phys Chem A 114:12952–12957
51. Jaffe RL, Smith GD (1996) J Chem Phys 105:2780–2788
52. Sinnokrot MO, Sherrill CD (2006) J Phys Chem A 110:10656–10668
53. Zhikol OA, Shishkin OV (2012) Int J Quantum Chem 112:3008–3017
54. Zhikol OA, Shishkin OV, Lyssenko KA, Leszczynski J (2005) J Chem Phys 122:144104–144108
55. Podeszwa R, Bukowski R, Szalewicz K (2006) J Phys Chem A 110:10345–10354
56. van der Avoird A, Podeszwa R, Szalewicz K, Leforestier C, van Harrevelt R, Bunker PR, Schnell M, von Helden G, Meijer G (2010) Phys Chem Chem Phys 12:8219–8240
57. Sinnokrot MO, Valeev EF, Sherrill CD (2002) J Am Chem Soc 124:10887–10893
58. Sinnokrot MO, Sherrill CD (2004) J Phys Chem A 108:10200–10207
59. Tauer TP, Sherrill CD (2005) J Phys Chem A 109:10475–10478
60. Sherrill CD, Takatani T, Hohenstein EG (2009) J Phys Chem A 113:10146–10159